Permian plume beneath Tarim from receiver functions

Lev Vinnik[1], Yangfan Deng[2], Grigoriy Kosarev[1], Sergey Oreshin[1], Larissa Makeyeva[1]

1. Institute of physics of the Earth, Russian Academy of Sciences, Moscow, Russia
2. State Key Laboratory of Isotope Geochemistry, Guangzhou Institute of Geochemistry, Chinese Academy of Sciences, Guangzhou 510640, China

Correspondence to: Yangfan Deng (Yangfandeng@gig.ac.cn) and Lev Vinnik (vinnik@ifz.ru)

Abstract

Receiver functions for the central Tien Shan and northern Tarim in central Asia reveal a pronounced depression on the 410-km discontinuity beneath the Permian basalts in Tarim. The depression may most likely be caused by elevated temperature. The striking spatial correlation between the anomaly of the MTZ and the Permian basalts suggests that both may be effects of the same plume. This relation can be reconciled with reconstructed positions of paleo-continents since the Permian by assuming that the mantle layer which translated coherently with the Tarim plate extended to a depth of 410 km or more. Alternatively, lithosphere and the underlying mantle are decoupled at a depth of ~ 200 km, but a cumulative effect of the Tarim plate motions since the Permian is by an order of magnitude less than predicted by the paleo-reconstructions. A similar explanation is applicable to the Siberian traps.

1. Introduction.

Theoretical considerations predict decoupling of the rigid lithosphere and the underlying ductile upper mantle (asthenosphere) at the lithosphere-asthenosphere boundary (Eaton et al., 2009). The depth to the lithosphere-asthenosphere boundary (LAB) ranges from a few tens kilometers for a young lithosphere to about 300 km for Precambrian cratons (e.g. Artemieva and Mooney, 2001). Another idea postulates that the layer which translates coherently with the continental plate (tectosphere) may extend to a depth of at least 400 km (Jordan, 1978).

Examples of successful application of the concept of tectosphere to geophysical data are few. We test this idea by comparing the locations of possible remnants of extinct mantle plumes in the mantle transition zone (MTZ) and the related basaltic outcrops at the Earth's surface.

Recently this test was applied to the Siberian Large Igneous Province (LIP). The Siberian traps present the result of gigantic basalt eruptions which took place near the Permo-Triassic boundary at about 250 Ma (Fedorenko et al., 1996). The analysis of structure of the mantle beneath the Siberian LIP was conducted with the aid of receiver function techniques that were applied to the recordings of seismograph station Norilsk (NRIL) within the Siberian LIP (Vinnik et al., 2017). This analysis has shown that the seismic boundary at the top of the MTZ with a standard depth of 410 km is depressed in the vicinity of NRIL by 10 km. The diagram of olivine - wadsleyite phase transition may account for this depression by assuming about 100 K increase of the temperature.

In the depth range from 350 to 410 km, the S velocity beneath the Siberian LIP is reduced by 4 – 5% (Vinnik and Farra, 2007) relative to IASP91 model (Kennett and Engdahl, 1991). This is a likely effect of about 1 vol % melt (Hier-Majumder and Courtier, 2011) which is unusual for cratons. Another low-velocity layer is found in the depth interval from 460 to 500 km. Previously this layer was found in the vicinities of several hot–spots (e.g., Vinnik et al., 2012). The low S-wave velocity coincides in depth with the abrupt decrease of the solidus temperature of carbonated mantle (Keshav et al., 2011) and may also be related to melting. The Siberian Craton shifted in the last 250 Myr by about 2000 km to the east (Torsvik et al., 2008). The anomalies of the MTZ might preserve their position beneath the Siberian LIP in spite of the plate motion if they translated coherently with the Siberian plate.

A similar conclusion is obtained for Greenland by Kraft et al. (2018). Arrival times of P660s and P410s mode converted phases in P receiver functions (PRFs) were measured at 24 seismograph stations in central-eastern Greenland. In two regions corresponding to basaltic outcrops about 55 Myr old, the differential time between P660s and P410s seismic phases is

reduced by more than 2 s relative to IASP91 reference model. The 410-km discontinuity in these regions is depressed by more than 20 km. The depression can be explained by elevated temperature. The basaltic outcrops and the related temperature anomalies are likely related to the passage of Greenland over the Iceland hot-spot. This explanation is consistent with the concept of tectosphere and implies that the upper mantle beneath Greenland to a depth of at least 430 km translated coherently with the Greenland plate.

Here we describe a similar analysis for the central Tien Shan and Tarim in central Asia and discuss possible implications of these observations.

2. Seismic structure of the MTZ beneath the central Tien Shan and Tarim.

This section presents in condensed form the results of the recent seismic study (Kosarev et al., 2018) of the MTZ beneath the central Tien Shan and northern Tarim (Fig.1). The ongoing orogenesis in central Asia is a likely far-field effect of the India-Eurasia collision (Molnar and Tapponnier, 1975). Previous mountain-building episodes in the region of the Tien Shan took place in the Paleozoic (e.g., Windley et al., 1990), but for about 100 Myr prior to the onset of the present-day mountain building the lithosphere of the Tien-Shan was quiet. Tectonic activity resumed at about 25-20 Ma in the southern Tien Shan (Sobel and Dumitru, 1997) and at 11 Ma in the north (Bullen et al., 2001). The lithosphere of Tarim underthrusts the relatively weak lithosphere of the Tien Shan at a rate of about 20 mm/yr (Reigber et al., 2001).

Teleseismic recordings of 64 broad-band stations in Fig. 1 were low-pass filtered with a corner at 6s and transformed into PRFs. The PRFs were calculated by using the LQ coordinate system, where L is parallel to the principal motion direction of the P wave and Q is normal to L in the wave propagation plane. The Q components were deconvolved by the L components in time domain and stacked to reduce noise. In the context of our study the most important elements of the PRFs are P660s and P410s mode converted seismic phases. The 410-km and 660-km discontinuities mark the top and bottom of the MTZ and their depths are sensitive to the temperature and composition.

The times of P660s and P410s seismic phases depend not only on topography of the 660-km and 410-km discontinuities but also on volumetric velocity heterogeneities above the 410-km boundary. Separation of these two effects is the main problem of interpreting the observations of P660s and P410s phases. This problem is solved by calculating the time difference (differential time) between the arrivals of P660s and P410s phases. The ray paths of P660s and P410s phases in the crust and upper mantle are close to each other for the same seismic recording, and, as a result, the differential time is insensitive to the properties of the Earth's medium above the MTZ.

To detect P660s and P410s phases and to map the differential time, a large number of the PRFs should be stacked. One possibility is to apply a version of CCP (Common Conversion Point) stacking: to divide the Earth's surface into cells and to stack with appropriate move-out time corrections the PRFs, the projections of the conversion points of which fall into the same cell. However, the surface projections of the conversion points of P410s and P660s phases for the same recording are at different distances (around 1° and 2°, respectively) from the seismograph station, and the set of PRFs thus selected for the detection of P410s phase may differ from that for P660s phase. Then the differential time of stacked P660s and P410s phases can be affected by lateral heterogeneity of the crust and mantle above the MTZ. This can be avoided by locating the conversion points in the middle of the MTZ (at a depth of 535 km) and stacking those PRFs, the projections of the conversion points of which are located within the same cell. Then P410s and P660s phases for each cell are detected in the same set of PRFs and the effect of lateral heterogeneity above the 410-km discontinuity is minimized.

Epicenters of seismic events of sufficient magnitude in a distance range from 35° to 90° are abundant in a broad azimuth range. Surface projections of the conversion points at a depth of 535 km cover the area between 38°N and 44°N and between 72°E and 82°E. The cells were chosen in the form of a rectangular box. The size of the box affects lateral resolution and, through the number of stacked PRFs, accuracy of the estimates of the differential time. The individual PRFs were visually inspected and only those of the best quality were stacked. The optimum size of the

box (2° for NS and EW or 220 km and 160 km, respectively) was found by trial and error. The largest number of the stacked PRFs exceeds 1750, the smallest is 48 (Table 1). These numbers are sufficient for a robust detection of P660s and P410s phases (see example in Fig. 2). The accuracy of the estimates of the differential time (confidence interval of 66%) which was determined by bootstrap resampling (Efron, Tibshirani, 1991) is typically 0.2 s. For most boxes the residuals of the differential time with respect to the IASP91 value (23.9 s) are on the order of a fraction of a second (Fig. 3). Large residuals (more than 1.0 s) are obtained for three boxes: (40° - 42°N, 76° - 78°E, +1.5 s), (40° - 42°N, 72° - 74°E, -1.1 s) and (38° - 40°N, 80° - 82°E, -1.5 s). Further on these boxes are referred as a, b and c. The resulting anomalies of thickness of the MTZ for a, b and c are +15 km, -11 km, and -15 km, respectively. These anomalies are located beneath the south-central Tien Shan, Fergana Basin and Tarim. We note that while the number of stacked PRFs for c is minimal (48), quality of the PRFs (signal-noise ratio) in this box is very high and the accuracy of the differential time is comparable with the other boxes.

The further analysis (Kosarev et al., 2018) demonstrates that the increased thickness of the MTZ in a is the effect of an uplift of the 410-km discontinuity and a depression of the 660-km discontinuity. The MTZ might be cooled by a detached and sinking mantle lithosphere. The thinned MTZ in b and c is the effect of a depressed 410-km discontinuity and a stable 660-km discontinuity. The depressed 410-km discontinuity beneath b and c is likely a result of a temperature anomaly of about +100°C. The elevated temperature in b may be related to a plume which is responsible for small-scale basaltic volcanism in the Tien Shan from 72 Ma to 60 Ma. Possible origin of the anomaly in c (Tarim) is discussed in next Section.

3. Possible origin of the anomalous MTZ beneath Tarim.

Tarim can be characterized as an Archean craton (Yuan et al., 2004) with a complex evolutional history (Zhang et al., 2013; Deng et al., 2017). In the Permian, basalts with the areal extent of about 200000 km^2 erupted in the west of the Tarim basin (Fig. 4). The thickness of basalt reaches 800 m. The age span of the magmatism extends from about 292 Ma to 272 Ma

with two peaks at 279 Ma and 289 Ma (Wei et al., 2014). The magmatism is interpreted as plume-induced (Zhang et al., 2010; Xu et al., 2014). Evidence for the mantle plume beneath Tarim includes the large volume of the Permian mafic rocks, OIB-like trace element signatures, Permian crustal doming and the high zircon saturation temperatures (Zhang et al., 2008, 2010). No magmatic activity is known after the Permian (Zhang et al., 2013; Deng et al., 2017).

Fig. 4 demonstrates a striking spatial correlation of the depressed 410-km discontinuity and the Permian magmatic province in Tarim, with implication of a causal relation between them. An alternative interpretation suggests that the topography on the 410-km discontinuity, though spatially correlated with the Permian basalts is caused by another, relatively young plume. However, this seems unlikely, as recently erupted (post-Permian) basalts are unknown in Tarim. The depressed 410-km discontinuity and the stable 660-km discontinuity are typical for hotspots and plumes (e.g. Du et al., 2006), though there are some exceptions (e.g. Vinnik et al., 2012). The stable depth of the 660-km discontinuity is either the result of a zero temperature anomaly at the base of the MTZ or an effect of two phase transitions at nearly the same depth but with opposite Clapeyron slopes (Hirose, 2002).

The assumed causal relation between the Permian basalts and the present-day anomaly implies that the anomaly at a depth of ~400 km may exist for ~300 Myr. To check this possibility we calculated the temperature for 1D conductive medium by using the well known expression (e.g., Zharkov et al., 1969) $T(r,t) = Q \exp(-r^2/4\alpha t)/2\sqrt{\pi\alpha t}$, where T is temperature, t is time, r is distance, α is diffusivity, Q is constant, and the initial temperature anomaly distribution is taken in the form of δ-function at $r = 0$ and $t = 0$. The diffusivity α is taken equal to 32 km^2/m.y. (e.g., Morgan and Sass, 1984). The results (Fig.5a) demonstrate that the temperature anomaly in the time interval of 300 m.y. (between 100 m.y. and 400 m.y.) is halved. The maximum temperature anomaly in plumes is ~300 ±100°C (Campbell, 2005), which means that the temperature anomaly after 300 m.y. may be around 150°C, close to the seismic estimate. A

comparable result is obtained for 2D conductive medium (Fig. 5b). These calculations suggest that the thermal anomaly at a depth of 400 km may survive for a few hundred million years.

It is also possible that the anomalous depth of the 410-km discontinuity is an effect of anomalous composition. The pressure of the phase transition in $(Mg,Fe)_2SiO_4$ depends on the Mg content (Mg#) relative to Fe (Fei and Bertka, 1999). Increasing Mg# from 89 to 92 results in up to 10-km deepening of the 410-km discontinuity (Schmerr and Garnero, 2007). The depleted composition and increased Mg# are commonly interpreted as effects of melting (e.g., Boyd, 1989).

Relative positions of the present-day thermal anomaly in the MTZ and the Permian basalt eruptions depend on plate motions in the last ~300 Myr. Reconstruction of positions of old continents is difficult for the time exceeding the age of the oldest hot-spot trails (130 Ma). There are abundant paleomagnetic data for the earlier times, but they do not constrain paleo-longitudes. The motions of Tarim are constrained by paleomagnetic data. According to Zhao et al. (1996) Tarim might be attached to Eurasia since the Late Paleozoic time, and there are paleomagnetic indications of displacements of Tarim relative to Eurasia after the Cretaceous, apparently owing to the India-Eurasia collision (Zhao et al., 1996). The uncertainty of the paleoreconstructions for the Mesozoic can be minimized by selecting Africa as a reference continent that was most stable longitudinally (Torsvik et al. 2008). In this reference frame the Siberian traps shifted to the east by nearly 2000 km since they were erupted at 250 Ma (Torsvik et al., 2008). On the assumption that Tarim and the Siberian craton were parts of the same continental plate in the past 300 Myr, 2000 km can be used as a rough estimate of the shift of Tarim.

The spatial correlation between the anomaly in the MTZ and the basalt eruptions in Tarim (Fig. 4) in spite of the shift of the Tarim craton to the east and north-east by a few thousand kilometers is possible if the layer which translates coherently with the plate includes the top of the MTZ. Alternatively this is possible without the recourse to the deep tectosphere, if the

available paleo-reconstructions for Asia are too rough and the actual shift of Tarim is by an order of magnitude less than predicted. This would also be true for the Siberian traps.

4.Conclusions

The striking spatial coincidence of the Permian basalts and a depression on the 410-km discontinuity beneath Tarim (Fig. 4) suggests that both may be related to the same mantle plume. This relation allows a dual interpretation. Recent reconstructions (Torsvik et al., 2008) demonstrate a shift of Tarim of about 2000 km in the past 300 Myr. Then the observed relation between the deep and shallow features can be explained by a coherent translation of the crust and mantle to a depth of 430 km. Alternatively the spatial coincidence of the deep and shallow features is possible without the recourse to the deep tectosphere if the actual shift of Tarim is by an order of magnitude less than predicted by the reconstructions. Practically similar conclusions would apply to the Permo-Triassic traps of the Siberian Craton.

Acknowledgment

This study was supported by the joint project between Russian Foundation for Basic Research (RFBR, grant 17-55-53-117) and National Natural Science Foundation of China (NSFC, grant 41611530695), the Strategic Priority Research Program (B) of the Chinese Academy of Sciences (grant XDB18000000). The authors appreciate comments from Dr. R. Porritt and an anonymous reviewer.

References

Artemieva, I. M., and Mooney, W. D.: Thermal thickness and evolution of Precambrian lithosphere: a global study, *Journal of Geophysical Research: Solid Earth*, *106*(B8), 16387-16414, 2001

Boyd, F.R.: Compositional distinction between oceanic and cratonic lithosphere, *Earth Planet. Sci. Lett.*, *96*, 15-26, 1989.

Bullen, M. E., Burbank, D. W., Garver, J. I., and Abdrakhmatov, K. Y.: Late Cenozoic tectonic evolution of the northwestern Tien Shan: New age estimates for the initiation of mountain building, *Geological Society of America Bulletin*, *113*(12), 1544-1559, 2001.

Campbell, I. H.: Large igneous provinces and the mantle plume hypothesis, *Elements*, *1*(5), 265-269, 2005.

Deng, Y., Levandowski, W., and Kusky, T.: Lithospheric density structure beneath the Tarim basin and surroundings, northwestern China, from the joint inversion of gravity and topography, *Earth and Planetary Science Letters*, *460*, 244-254, 2017.

Du, Z., Vinnik, L. P., and Foulger, G. R.: Evidence from P-to-S mantle converted waves for a flat “660-km” discontinuity beneath Iceland, *Earth and Planetary Science Letters*, *241*(1-2), 271-280, 2006.

Eaton, D. W., Darbyshire, F., Evans, R. L., Grütter, H., Jones, A. G., and Yuan, X.: The elusive lithosphere–asthenosphere boundary (LAB) beneath cratons, *Lithos*, *109*(1-2), 1-22, 2009.

Efron, B., Tibshirani, R.: Statistical data analysis in the computer age, *Science*, 253, 390-395, 1991.

Fedorenko, V. A., Lightfoot, P. C., Naldrett, A. J., Czamanske, G. K., Hawkesworth, C. J., Wooden, J. L., and Ebel, D. S.: Petrogenesis of the flood-basalt sequence at Noril'sk, north central Siberia, *International Geology Review*, *38*(2), 99-135, 1996.

Fei, Y., and Bertka, C. M.: Phase transitions in the Earth’s mantle and mantle mineralogy, *Mantle petrology: field observations and high pressure experimentation*, *6*, 189-207, 1999.

Jordan, T. H.: Composition and development of the continental tectosphere, *Nature*, *274*(5671), 544, 1978.

Hier-Majumder, S., and Courtier, A.: Seismic signature of small melt fraction atop the transition zone, *Earth and Planetary Science Letters*, *308*(3-4), 334-342, 2011.

Hirose, K.: Phase transitions in pyrolitic mantle around 670 - km depth: Implications for upwelling of plumes from the lower mantle, *Journal of Geophysical Research: Solid Earth*, *107*(B4), 2002.

Kennett, B.L.N. and Engdahl, E.R.: Traveltimes for global earthquake location and phase identification. *Geophysical Journal International*, *105*(2), 429-465, 1991.

Keshav, S., Gudfinnsson, G.H., and Presnall, D.C.: Melting phase relations of simplified carbonated peridotite at 12 – 26 GPa in the systems CaO – MgO – SiO_2 – CO_2 and CaO – MgO – Al_2O_3 – SiO_2 – CO_2: highly calcic magmas in the transition zone of the Earth. *Journal of Petrology*, *52*, 2265-2291, 2011.

Kosarev, G., Oreshin, S., Vinnik, L., and Makeyeva, L.: Mantle transition zone beneath the central Tien Shan: Lithospheric delamination and mantle plumes, *Tectonophysics*, *723*, 172-177, 2018.

Kraft, H. A., Vinnik, L., and Thybo, H.: Mantle transition zone beneath central-eastern Greenland: Possible evidence for a deep tectosphere from receiver functions, *Tectonophysics*, *728*, 34-40, 2018.

Molnar P., and Tapponnier P.: Cenozoic tectonics of Asia: effects of a continental collision, *Science*, 189, 419-426, 1975.

Morgan, P. and Sass, S.: Thermal regime of the continental lithosphere, *Journal of Geodynamics* *1*, 143-166, 1984.

Reigber, C., Michel, G., Galas, R., Angermann, D., Klotz, J., Chen, J., Papschev, A., Arslanov, R., Tzurkov, V. and Ishanov, M.: New space geodetic constraints on the distribution of deformation in Central Asia. *Earth and Planetary Science Letters*, *191*(1-2), 157-165, 2001.

Schmerr, N., and Garnero, E. J.: Upper mantle discontinuity topography from thermal and chemical heterogeneity, *Science*, *318*(5850), 623-626, 2007.

Sobel, E. R., and Dumitru, T. A.: Thrusting and exhumation around the margins of the western Tarim basin during the India–Asia collision, *Journal of Geophysical Research: Solid Earth*, *102*(B3), 5043-5063, 1997.

Torsvik, T. H., Steinberger, B., Cocks, L. R. M., and Burke, K.: Longitude: linking Earth's ancient surface to its deep interior, *Earth and Planetary Science Letters*, *276*(3-4), 273-282, 2008.

Vinnik, L., and Farra, V.: Low S velocity atop the 410-km discontinuity and mantle plumes, Earth Planet. *Sci. Lett.*, *262*, 398-412, 2007.

Vinnik, L., Silveira, G., Kiselev, S., Farra, V., Weber, M., and Stutzmann, E.: Cape Verde hotspot from the upper crust to the top of the lower mantle, *Earth and Planetary Science Letters*, *319*, 259-268, 2012.

Vinnik, L. P., Oreshin, S. I., and Makeyeva, L. I.: Siberian traps: Hypotheses and seismology data, *Izvestiya, Physics of the Solid Earth*, *53*(3), 332-340, 2017.

Wei, X., Xu, Y.-G., Feng, Y.-X., Zhao, J.-X.: Plume-lithosphere interaction in the generation of the Tarim large igneous province, NW China: geochronological and geochemical constraints. *American Journal of Science*, 314, 314-356, 2014.

Windley, B. F., Allen, M. B., Zhang, C., Zhao, Z. Y., and Wang, G. R.: Paleozoic accretion and Cenozoic redeformation of the Chinese Tien Shan range, central Asia. *Geology*, *18*(2), 128-131, 1990.

Xu, Y.-G., Wei, X., Luo, Z.-Y., Liu, H.-Q., and Cao, J.: The Early Permian Tarim Large Igneous Province: main characteristics and a plume incubation model. *Lithos*, *204*, 20–35, 2014.

Yuan, C., Sun, M., Yang, J., Zhou, H., and Zhou, M.-F.: Nb-depleted, continental rift-related Akaz metavolcanic rocks (West Kunlun): implication for the rifting of the Tarim Craton from Gondwana. *Geological Society, London, Special Publications*, *226*(1), 131-143, 2004.

Zhang, C., Li, X., Li, Z., Ye, H., and Li, C.: A permian layered intrusive complex in the western tarim block, northwestern China: Product of a Ca. 275-ma mantle plume? *The Journal of Geology*, 116, 269-287, 2008.

Zhang, C.-L., Xu, Y.-G., Li, Z.-X., Wang, H.-Y., and Ye, H.-M.: Diverse Permian magmatism in the Tarim Block, NW China: Genetically linked to the Permian Tarim mantle plume? *Lithos*, 119, 537-552, 2010.

Zhang, C.-L., Zou, H.-B., Li, H.-K., and Wang, H.-Y.: Tectonic framework and evolution of the Tarim Block in NW China. *Gondwana Research, 23*(4), 1306-1315, 2013.

Zhao, X., Coe, R.S., Gilder, S.A. and Frost, G.M.: Paleomagnetic constraints on the palaeogeography of China: implications for Gondwanaland, *Australian Journal of Earth Sciences, 43*, 643-672, 1996.

Zharkov, V.N., Pan'kov, V.L., Kalachnikov, A.A. and Osnach, A.I. Introduction in the physics of the Moon , "Nauka", Moscow, 1969. (in Russian).

Figure captions

Figure 1. Topographic map of the study region and the seismograph network.

Figure 2. Stacked PRFs for the box with the coordinates: 38 N, 40N, 80 E and 82 E. Trial conversion depths in kilometers for each trace are shown on the left-hand side. The detected P410s and P660s phases are marked by arrows. Note that the largest amplitudes of P410s and P660s phases are observed at appropriate trial depths (around 400-500 km and 600=700 km, respectively).

Figure 3. Residuals of the differential time between P660s and P410s phases in seconds relative to IASP91. Strongly anomalous boxes are in south-central Tien Shan (1.5 s, blue, a), Fegana basin (-1.1 s, red, b) and Tarim (-1.5 s, red, c). Light shading indicates elevations greater than 1500 m, intermediate shading elevations greater than 3000 m.

Figure 4. Superiposed Permian basalts in Tarim (orange) and the anomalous region on the 410-km discontinuity.

Figure 5. Temperature anomaly distributions in 1D (a) and 2D (b) conductive media with an interval of 300 million years.

Table 1. Numbers of piercing points in the boxes in Fig. 3.

lat1	lat2	lon1	lon2	number of pp
38	40	72	74	132
38	40	74	76	267
38	40	76	78	402
38	40	78	80	96
38	40	80	82	48
40	42	72	74	414
40	42	74	76	1130
40	42	76	78	1512
40	42	78	80	616
40	42	80	82	322
42	44	72	74	317
42	44	74	76	757
42	44	76	78	1766
42	44	78	80	533
42	44	80	82	332
44	46	74	76	120

Figure 1

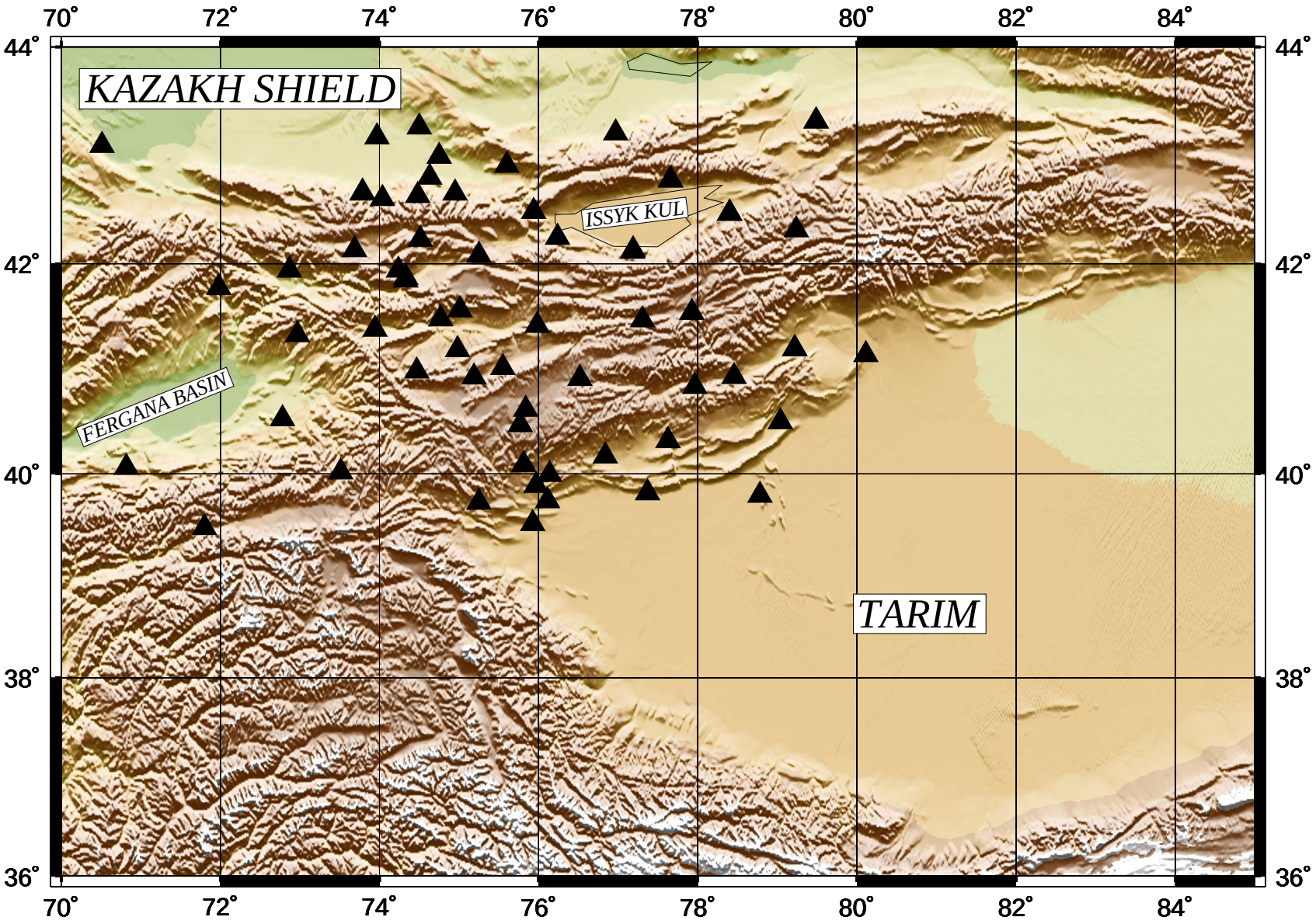
70°
72°
74°
76°
78°
80°
82°
84°
44°
42°
40°
38°
36°
KAZAKH SHIELD
ISSYK KUL
FERGANA BASIN
TARIM

Figure 2

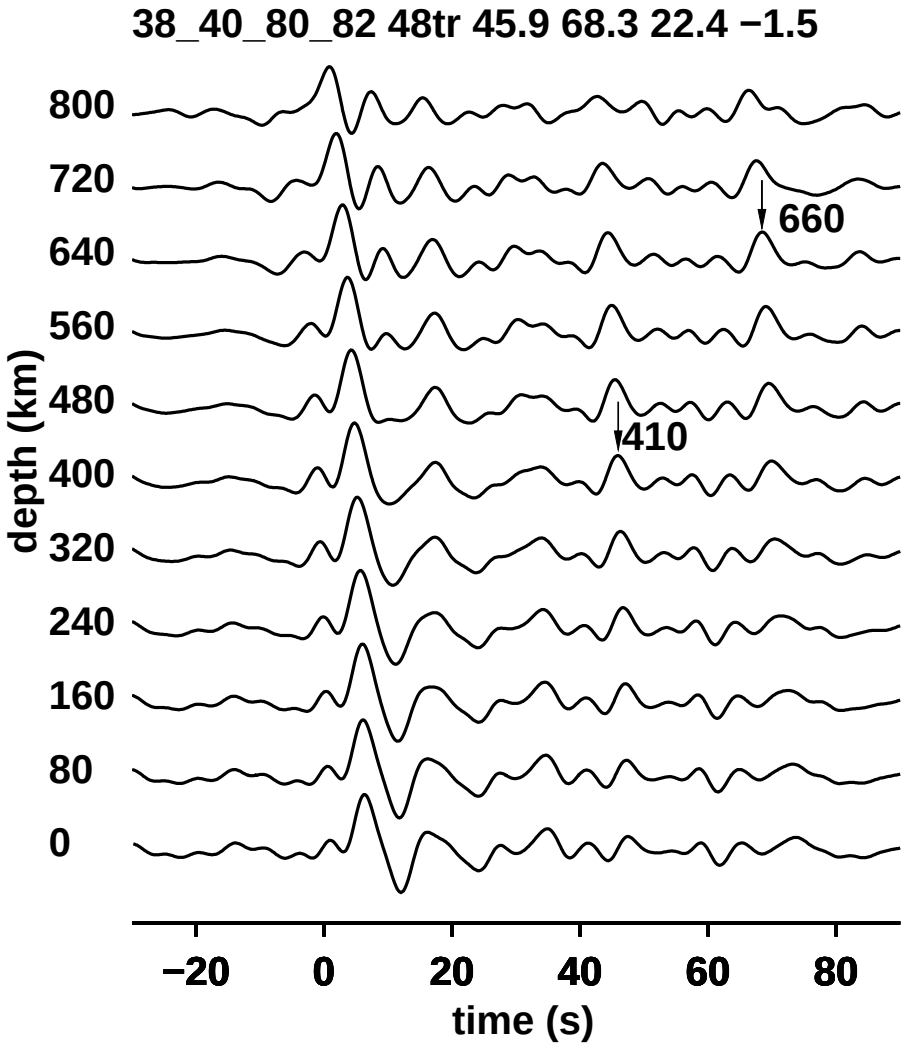
38_40_80_82 48tr 45.9 68.3 22.4 −1.5
800
720
640
560
480
400
320
240
160
80
0
660
410
depth (km)
−20
0
20
40
60
80
time (s)

Figure 3

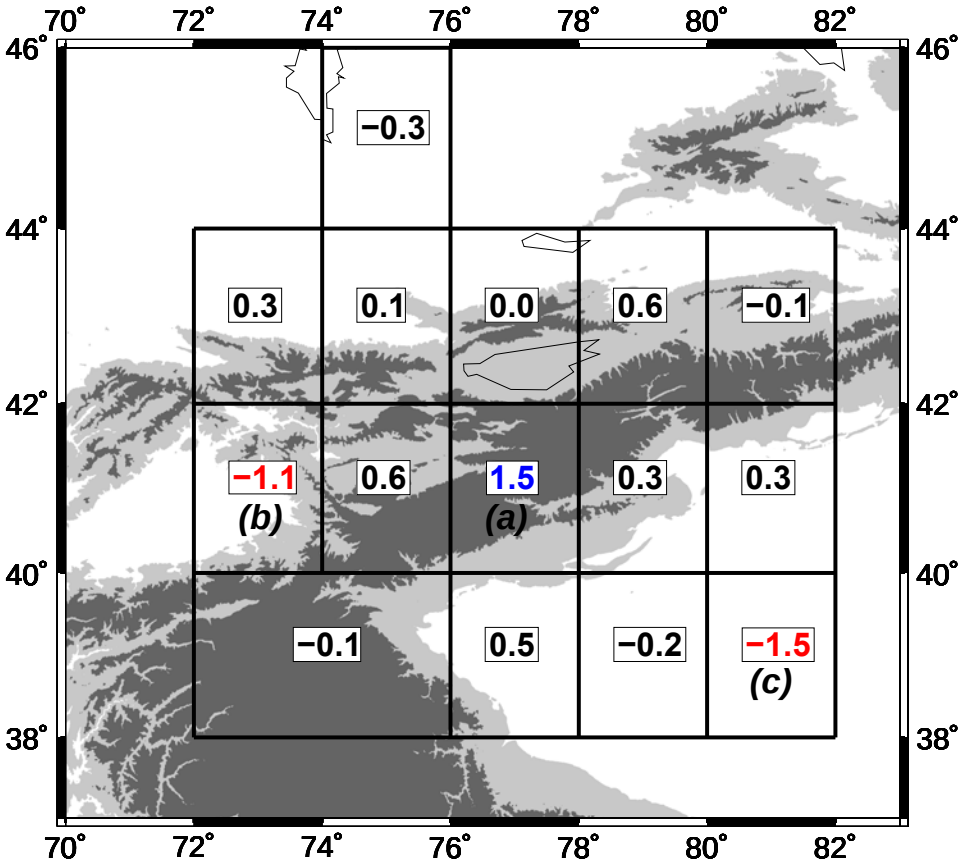
70°
72°
74°
76°
78°
80°
82°
46°
44°
42°
40°
38°
−0.3
0.3
0.1
0.0
0.6
−0.1
−1.1
(b)
0.6
1.5
(a)
0.3
0.3
−0.1
0.5
−0.2
−1.5
(c)

Figure 4

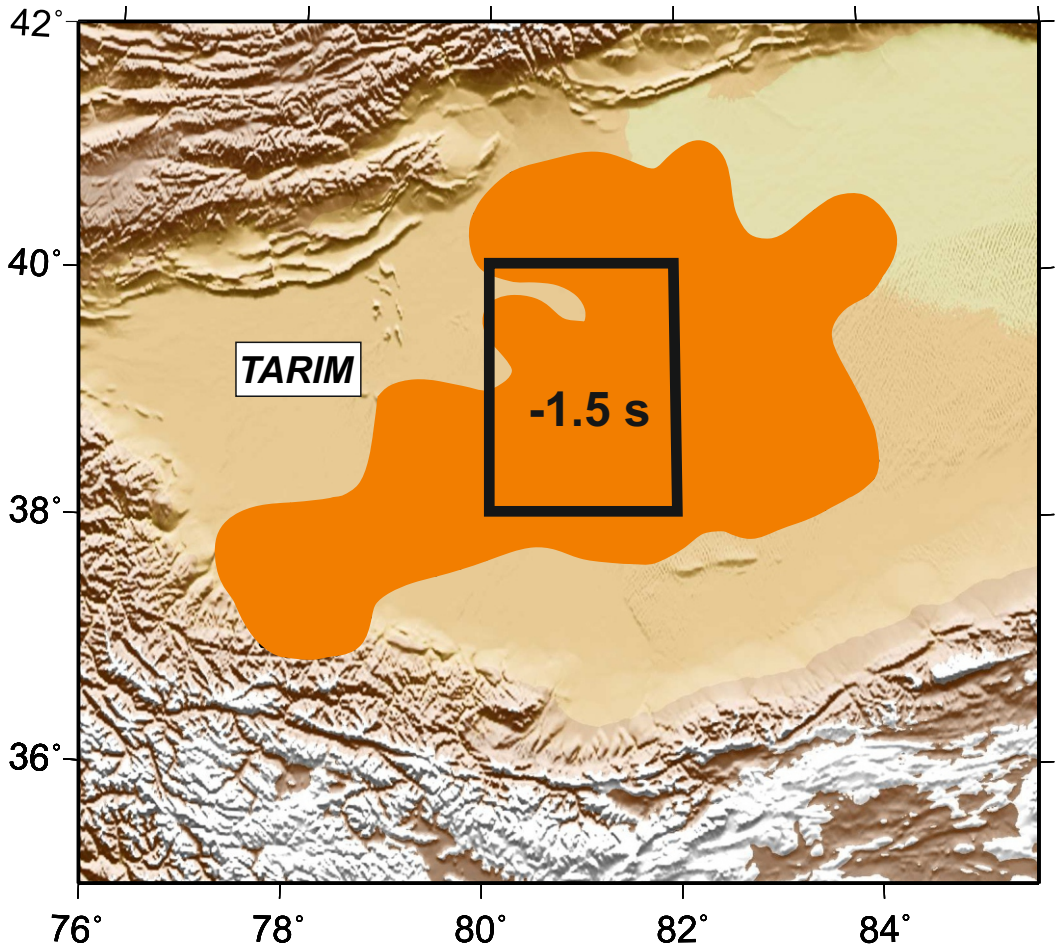

Figure 5

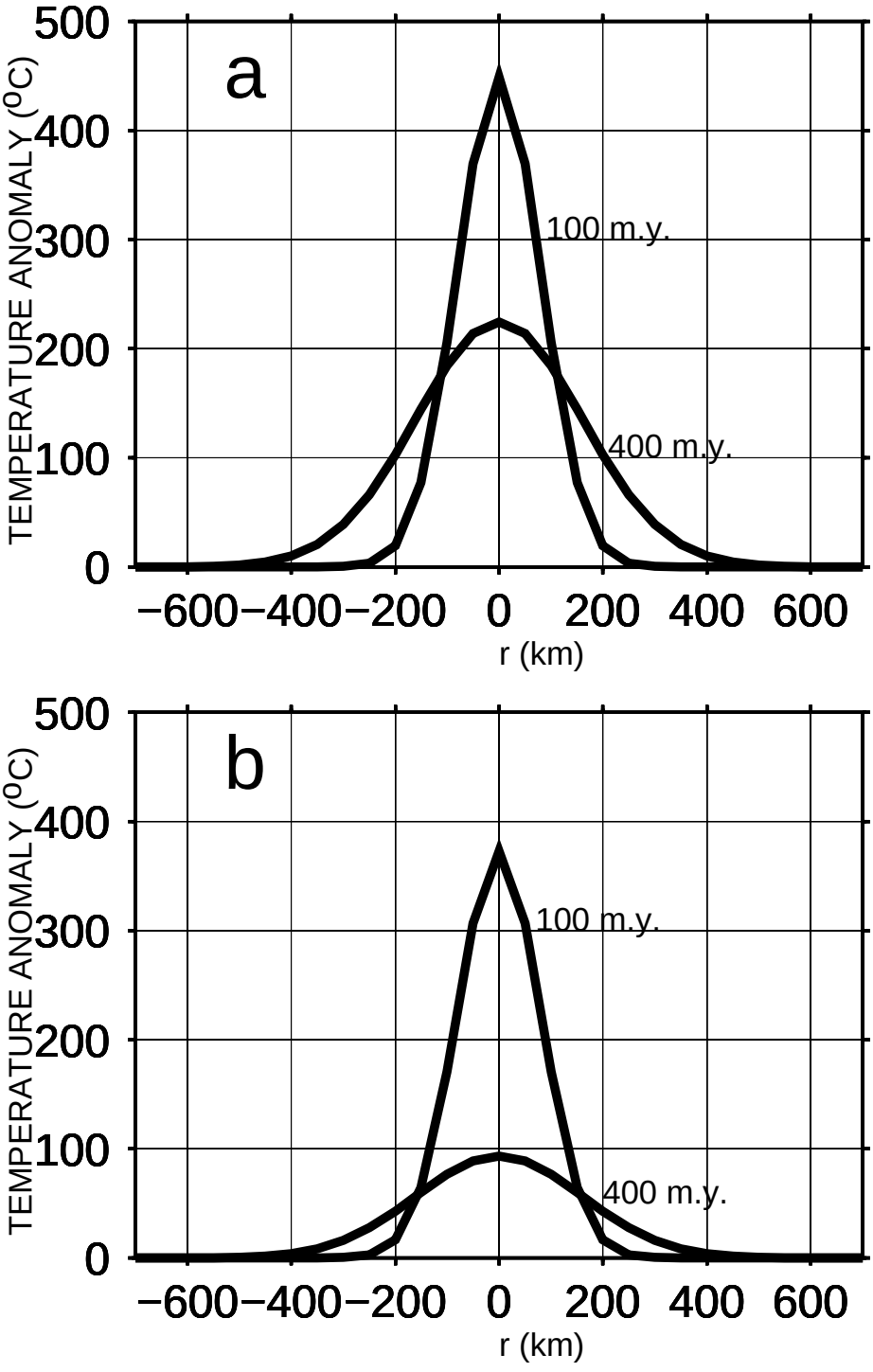
a
b
100 m.y.
400 m.y.
TEMPERATURE ANOMALY (°C)
r (km)
500
400
300
200
100
0
−600
−400
−200
0
200
400
600